Inorganic Chemistry

Article

pubs.acs.org/IC

A(II)GeTeO$_6$ (A = Mn, Cd, Pb): Non-Centrosymmetric Layered Tellurates with PbSb$_2$O$_6$-Related Structure

Sun Woo Kim,[†] Zheng Deng,[‡] Shuang Yu,[‡] Haricharan Padmanabhan,[§] Weiguo Zhang,[∥] Venkatraman Gopalan,[§] Changqing Jin,[‡] and Martha Greenblatt*[,†]

[†]Department of Chemistry and Chemical Biology, Rutgers, 610 Taylor Road, Piscataway, New Jersey 08854, United States

[‡]Beijing National Laboratory for Condensed Matter Physics, Institute of Physics, Chinese Academy of Sciences, Beijing 100190, China

[§]Department of Materials Science and Engineering, Pennsylvania State University, University Park, Pennsylvania 16802, United States

[∥]Department of Chemistry, University of Houston, 112 Fleming Building, Houston, Texas 77204, United States

Supporting Information

ABSTRACT: A(II)GeTeO$_6$ (A = Mn, Cd, Pb), new non-centrosymmetric (NCS) honeycomb-layered tellurates, were synthesized and characterized. A(II)GeTeO$_6$ (A = Mn, Cd, Pb) crystallize in trigonal space group *P*312 (No. 149) of edge-sharing Ge^{4+}O$_6$ and Te^{6+}O$_6$ octahedra, which form honeycomb-like-layers in the *ab*-plane with A(II) (A = Mn, Cd, Pb) cations located between the layers. Their crystal structures are PbSb$_2$O$_6$-related, and the ordering of Ge^{4+} and Te^{6+} in octahedral environment breaks the inversion symmetry of the parent PbSb$_2$O$_6$ structure. The size of A(II) cation in six coordination is an important factor to stabilize PbSb$_2$O$_6$-based structure. Temperature-dependent optical second harmonic generation measurements on A(II)GeTeO$_6$ confirmed non-centrosymmetric character in the entire scanned temperature range (0 to 600 °C). The materials exhibit a powder SHG efficiency of ∼0.37 and ∼0.21 times of KH$_2$PO$_4$ for PbGeTeO$_6$ and CdGeTeO$_6$, respectively. Magnetic measurements of MnGeTeO$_6$ indicate anti-ferromagnetic order at $T_N \approx 9.4$ K with Weiss temperature of −22.47 K.

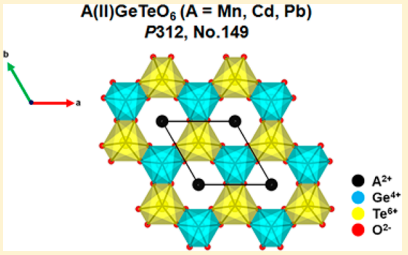

INTRODUCTION

Non-centrosymmetric (NCS) oxide materials have been studied extensively due to their important physical properties including ferroelectricity, piezoelectricity, pyroelectricity, multiferroicity, magnetoelectricity, and second harmonic generation (SHG).[1−5] Designing new NCS oxide materials with optimal characteristic is still challenging, and several approaches to break inversion symmetry have been investigated experimentally and theoretically; for example: (1) the combination of second-order Jahn−Teller (SOJT) d^0 cations (Ti^{4+}, Nb^{5+}, W^{6+}, etc.) and lone-pair cations (Bi^{3+}, Se^{4+}, Te^{4+}, etc.), which present asymmetric coordination environment and induce inversion symmetry breaking[6−9] and (2) oxygen octahedral rotation in layered perovskites (Ruddlesden−Popper or Dion−Jacobson phases), which recently have been confirmed experimentally.[10,11]

The PbSb$_2$O$_6$-type materials (general formula, ABB′O$_6$) exhibit a layered honeycomb structure (centrosymmetric (CS) space group, $P\bar{3}1m$, No. 162) with edge-sharing B/B′O$_6$ octahedra separated by A(II) cations (AO$_6$ octahedra).[12] Interesting magnetic behavior such as high anti-ferromagnetic (AFM) transition temperature was observed in magnetic cation-substituted PbSb$_2$O$_6$-related phases, for example, A(II)-As$_2$O$_6$ (A = Mn, Co, Ni, Pd)[13−16] and SrRu$_2$O$_6$.[17,18] Previously, we demonstrated that chemical modification of PbSb$_2$O$_6$-type structures by B/B′ cation ordering or rearrangement lead to breaking of the inversion symmetry. We observed two different NCS crystal structures: (1) B/B′ cation ordered with octahedral environment (e.g., SrGeTeO$_6$, *P*312, No. 149)[19] and (2) B/B′ cations randomly distributed with trigonal prismatic environment (e.g., SrMnTeO$_6$ and PbMnTeO$_6$, $P\bar{6}2m$, No. 189).[20,21] In addition, from the superstructure of PbSb$_2$O$_6$-related materials (general formula, A(III)BB′O$_6$), we were able to observe two different CS crystal structures depending on the degree of B/B′ cation ordering: (1) B/B′ cations are partially ordered with octahedral environment (e.g., BiCrTeO$_6$ and BiFeTeO$_6$, $P\bar{3}1c$, No. 163)[22,23] and (2) B/B′ cations fully ordered with distorted octahedral environment (e.g., BiMnTeO$_6$, P2$_1$/*c*, No. 14).[23] These findings suggest that a variety of compositional modifications in PbSb$_2$O$_6$-related materials are possible, which would help to design new NCS oxide material with optimal characteristics.

In the present study, we explored new compositional modifications of PbSb$_2$O$_6$-related phases to find new NCS materials with interesting and useful physical properties, and we report the successful synthesis and characterization of new NCS layered honeycomb tellurates, A(II)GeTeO$_6$ (A = Mn, Cd, Pb).

Received: April 24, 2017
Published: July 24, 2017

DOI: 10.1021/acs.inorgchem.7b01013
Inorg. Chem. 2017, 56, 9019−9024

EXPERIMENTAL SECTION

Reagents. $MnCO_3$ (Aldrich, 99.995%), CdO (Alfa Aesar, 99.998%), $PbCO_3$ (Aldrich, 99.99+%), GeO_2 (Alfa Aesar, 99.999%), and $H_2TeO_4{\cdot}2H_2O$ (Alfa Aesar, 99+%) were used without any further purification. Amorphous TeO_3 was prepared by heating $H_2TeO_4{\cdot}2H_2O$ at 400 °C for 12 h in air.[24]

Synthesis. Polycrystalline A(II)$GeTeO_6$ (A = Mn, Cd, Pb) were prepared by a conventional solid-state reaction. For the synthesis of $MnGeTeO_6$, stoichiometric amounts of $MnGeO_3$ (0.2634 g, 1.5 mmol) and TeO_3 (0.2634 g, 1.5 mmol) were ground and pressed into a pellet. The pellet was placed in an alumina crucible and treated for 12 h at 700 °C in air, then reground into fine powder, pressed into a pellet again, and heated to 700 °C for 12 h, then cooled to room temperature (the heating and cooling rate was 200 °C/h, respectively). $MnGeO_3$ was prepared with stoichiometric amounts of $MnCO_3$ and GeO_2 at 1150 °C for 12 h in air. A(II)$GeTeO_6$ (A = Cd, Pb), was synthesized from stoichiometric amounts of CdO (0.1926 g, 1.5 mmol) or $PbCO_3$ (0.4008 g, 1.5 mmol), GeO_2 (0.1569 g, 1.5 mmol), and TeO_3 (0.2634 g, 1.5 mmol) by identical treatments as the Mn analogue. The final products, orange $MnGeTeO_6$, ivory $CdGeTeO_6$, and white $PbGeTeO_6$ polycrystalline powders were obtained. The purity of all materials was confirmed by powder X-ray diffraction (PXRD).

Powder X-ray Diffraction and Rietveld Refinement. A(II)-$GeTeO_6$ (A = Mn, Cd, Pb) were characterized by PXRD (Bruker-AXS D8-Advanced diffractometer with Cu Kα, λ = 1.5406 Å, 40 kV, 40 mA, step scan 10−100°/0.02°/10.5 s) for purity and phase identification. Diffraction data analysis and Rietveld refinement were performed with the TOPAS[25] and GSAS-EXPGUI software package.[26] The structural refinements for A(II)$GeTeO_6$ (A = Mn, Cd, Pb) were performed on PXRD data based on the $SrGeTeO_6$ structural model (*P*312, No. 149). The A atoms (A = Mn, Cd, Pb) are located at 1*a* (0, 0, 0), Ge atoms are at 1*f* (2/3, 1/3, 1/2), Te atoms are at 1*d* (1/3, 2/3, 1/2), and O atoms are at 6*l* (*x*, *y*, *z*) positions in *P*312. The Rietveld refinement plots of PXRD data for $MnGeTeO_6$ are shown in Figure 1, and for

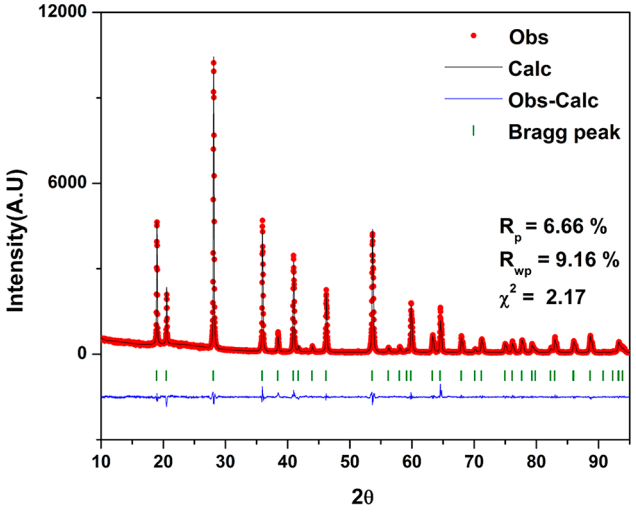

Figure 1. Rietveld refinement plots from PXRD data for $MnGeTeO_6$.

A(II)$GeTeO_6$ (A = Cd, Pb) they are in the Supporting Information, Figure S1, respectively. Crystallographic data, unit-cell parameters, atomic coordinates, and atomic displacement parameters are summarized in Table 1 and Table 2, respectively.

Second Harmonic Generation (SHG). Temperature dependence of optical SHG by A(II)$GeTeO_6$ (A = Mn, Cd, Pb) was obtained by measurements on polycrystalline pressed pellets in reflection geometry at normal incidence, with an 800 ± 20 nm fundamental input generated by a Ti:sapphire laser (Spectra-Physics, 80 fs pulses, 2 kHz frequency). The SHG signal was detected with a photomultiplier tube (Hamamatsu H7926). The samples were heated and cooled at a rate of 10.0 °C/min on a home-built heating stage. Powder SHG measurements, to quantify the SHG relative to the reference polycrystalline KH_2PO_4 (KDP), were also performed for A(II)-$GeTeO_6$ (A = Mn, Cd, Pb) at room temperature, on a modified Kurtz-NLO system[27] with a pulsed Nd:YAG laser of wavelength 1064 nm. A detailed description of the equipment and methodology has been reported elsewhere.[28] As powder SHG efficiency has been shown to be strongly dependent on particle size, the polycrystalline samples were ground and sieved into distinct particle size ranges (<20, 20−45, 45−63, 63−75, 75−90, >90 μm). The reference crystalline KDP was also ground and sieved into the same particle size ranges, to make relevant

Table 1. Crystallographic Data of A(II)$GeTeO_6$ (A = Mn, Cd, Pb)

source	laboratory X-ray
chemical formula	$MnGeTeO_6$; $CdGeTeO_6$; $PbGeTeO_6$
formula weight (g/mol)	351.15 ($MnGeTeO_6$)
	408.62 ($CdGeTeO_6$)
	503.41 ($PbGeTeO_6$)
temperature (K)	296
wavelength	Cu Kα, λ = 1.5406 Å
crystal system	trigonal
space group	*P*312 (No. 149)
unit cell dimensions	$a = b$ = 4.998 89(2) Å, c = 4.683 69(7) Å ($MnGeTeO_6$)
	$a = b$ = 5.035 99(1) Å, c = 4.845 95(4) Å ($CdGeTeO_6$)
	$a = b$ = 5.089 39(1) Å, c = 5.448 83(4) Å ($PbGeTeO_6$)
	$\alpha = \beta = 90°$, $\gamma = 120°$
volume (Å^3)	101.360(1) ($MnGeTeO_6$)
	106.434(1) ($CdGeTeO_6$)
	122.227(1) ($PbGeTeO_6$)
Z	1
density (calculated) (g/cm^3)	5.753 ($MnGeTeO_6$)
	6.375 ($CdGeTeO_6$)
	6.839 ($PbGeTeO_6$
χ^2, R_p, R_{wp}	2.17, 6.66, 9.16 ($MnGeTeO_6$)
	2.25, 6.84, 8.99 ($CdGeTeO_6$)
	1.98, 5.55, 7.72 ($PbGeTeO_6$)

Table 2. Atomic Coordinates and Atomic Displacement Parameters for A(II)$GeTeO_6$ (A = Mn, Cd, Pb)

		$MnGeTeO_6$			
atom	Wyck	*x*	*y*	*z*	U_{iso} (Å^2)
Mn(1)	1a	0	0	0	0.0011(3)
Ge(1)	1f	2/3	1/3	1/2	0.0016(9)
Te(1)	1d	1/3	2/3	1/2	0.0021(1)
O(1)	6l	0.3641(5)	0.0140(9)	0.2668(3)	0.0014(1)
		$CdGeTeO_6$			
atom	Wyck	*x*	*y*	*z*	U_{iso} (Å^2)
Cd(1)	1a	0	0	0	0.0028(5)
Ge(1)	1f	2/3	1/3	1/2	0.0018(2)
Te(1)	1d	1/3	2/3	1/2	0.0045(4)
O(1)	6l	0.3770(2)	0.0156(3)	0.2754(4)	0.0082(2)
		$PbGeTeO_6$			
atom	Wyck	*x*	*y*	*z*	U_{iso} (Å^2)
Pb(1)	1a	0	0	0	0.0023(7)
Ge(1)	1f	2/3	1/3	1/2	0.0018(6)
Te(1)	1d	1/3	2/3	1/2	0.0018(3)
O(1)	6l	0.3848(1)	0.0154(1)	0.2985(1)	0.0029(2)

DOI: 10.1021/acs.inorgchem.7b01013
Inorg. Chem. 2017, 56, 9019−9024

comparisons with the unknown SHG materials. No index matching fluid was used in any of the experiments.

Magnetic Measurements. The magnetic measurements for $MnGeTeO_6$ were performed with a commercial Quantum Design SQUID VSM Magnetometer. The direct-current (dc) magnetic susceptibility data were collected between $2 \leq T \leq 300$ K under an applied magnetic field of 1000 Oe. Isothermal magnetization curves were obtained for magnetic fields: $-7\ T \leq H \leq 7\ T$ at $T = 2$ and 300 K.

RESULTS AND DISCUSSION

Synthesis. Previously, Woodward et al. reported synthesis and crystal structure of $A(II)GeTeO_6$ (A = Sr, Ba).[19] The crystal structure of $SrGeTeO_6$ exhibits $PbSb_2O_6$-related structure with *P*312 space group, No. 149. In contrast, the crystal structure of $BaGeTeO_6$ (space group, *P*312, No. 149) shows doubling of *c*-axis with different coordination environment of cations; thus, it is not isostructural with $SrGeTeO_6$.[19] The difference of the two crystal structures can be attributed to the size of A cation in six coordination environment (Sr^{2+}: 1.18 Å vs. Ba^{2+}: 1.35 Å), and this result suggests that the size of A(II) cations may also play an important factor to stabilize the $PbSb_2O_6$-type structure. In the present study, we tried to substitute various divalent A cations (3d−4d transition metals and others) into the $PbSb_2O_6$ structure with *P*312 space group (see Supporting Information). $A(II)GeTeO_6$ (A = Mn, Cd, Pb) were successfully prepared, and the experimental results indicated that the effective octahedral size of A(II) cation should be larger than 0.8 Å to stabilize the $PbSb_2O_6$-based structure (Mn^{2+}: 0.83 Å, Cd^{2+}: 0.95 Å, and Pb^{2+}: 1.19 Å).

Structure. $A(II)GeTeO_6$ exhibit a two-dimensional crystal structure (space group (SG): *P*312, No. 149) consisting of edge-sharing $Ge(1)O_6$ and $Te(1)O_6$ octahedra, which form honeycomb-like layer in the *ab*-plane with A^{2+} cations (AO_6 octahedra) located between the layers (see Figure 2).

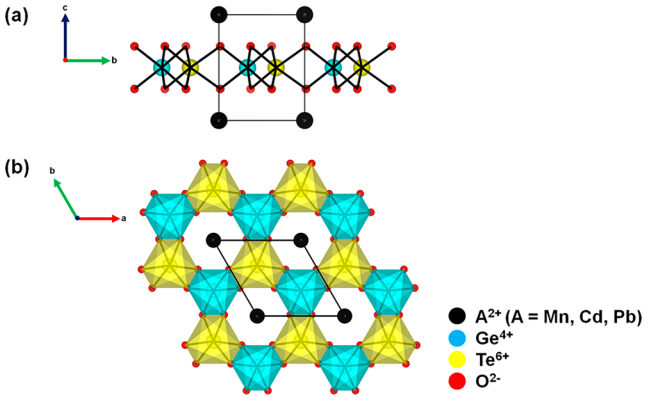

Figure 2. Crystal structure of the $A(II)GeTeO_6$ (A = Mn, Cd, Pb): (a) ball-and-stick diagram in the *bc* planes and (b) polyhedral representation in the *ab* planes.

Compared to the parent $PbSb_2O_6$ structure ($P\bar{3}1m$, No. 162), the cation ordering of Ge^{4+} and Te^{6+} in the octahedral environment induces a lower crystal symmetry and breaks the inversion symmetry to form an NCS structure (see Figure 3). The origin of such ordering could be attributed to the Coulombic repulsion of Ge^{4+}/Te^{6+} and their off centering in the edge-sharing octahedra.

As the size of A(II) cation increases (Mn^{2+}: 0.83 Å, Cd^{2+}: 0.95 Å, Pb^{2+}: 1.19 Å), the ratio of *c*/*a* in $A(II)GeTeO_6$ also increases (0.9369 for $MnGeTeO_6$, 0.9623 for $CdGeTeO_6$,

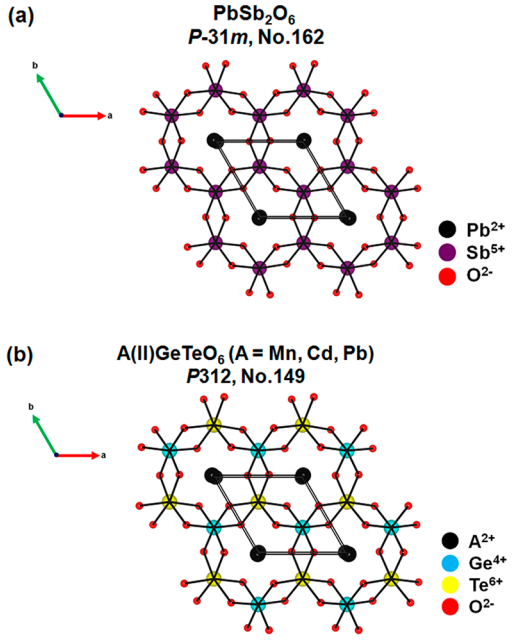

Figure 3. Comparison of ball-and-stick diagram for $PbSb_2O_6$-related materials: (a) $PbSb_2O_6$ in the *bc*-plane[12] and (b) $A(II)GeTeO_6$ (A = Mn, Cd, Pb) in the *bc*-plane (this work).

1.0706 for $PbGeTeO_6$). The Ge(1)−O(1) bond distances in $A(II)GeTeO_6$ range between 1.8809(1) and 1.9008(1) Å, and the Te(1)−O(1) bond distances range between 1.9835(1) and 1.9913(1) Å. The bond angles of Ge(1)−O(1)−Te(1) range between 95.6920(6)° and 98.5564(4)°; the bond angles of Mn(1)−O(1)−Ge(1) and Mn(1)−O(1)−Te(1) in $MnGeTeO_6$ are 131.1152(3)° and 125.9436(3)°, respectively. The bond distances of A(1)−O(1) in the AO_6 octahedra are 2.1799(2) Å for $MnGeTeO_6$, 2.2898(1) Å for $CdGeTeO_6$, and 2.5172(1) Å for $PbGeTeO_6$ with six equivalent distances, respectively. It is noteworthy that six equivalent distances of Pb−O in $PbGeTeO_6$ indicate that the Pb^{2+} cation is nonstereo active, as it was also observed in other Pb^{2+}-containing layered oxides.[12,21] Selected bond distances and angles for $A(II)GeTeO_6$ are summarized in the Table 3. Bond valence sum calculations[29,30] resulted in values of 2.09, 2.12, 1.94, 3.97−4.19, and 5.77−5.89 for Mn^{2+}, Cd^{2+}, Pb^{2+}, Ge^{4+}, and Te^{6+}, respectively (see Table 3).

Second Harmonic Generation (SHG). The SHG intensity as a function of temperature for $A(II)GeTeO_6$ (A = Mn, Cd, Pb) is shown in Figure 4. Finite SHG intensity was observed over the entire measured temperature range, confirming that $A(II)GeTeO_6$ are NCS. The samples were not heated above 600 °C in the SHG experiment, as a thermogravimetric analysis (TGA) for $A(II)GeTeO_6$ (A = Mn, Cd, Pb) at 1000 °C in air indicated the decomposition of the compounds (see Supporting Information, Figures S3 and S4).

We performed temperature-dependent SHG measurements on $A(II)GeTeO_6$ (A = Mn, Cd, Pb) to determine possible NCS-to-CS phase transition and to get a better understanding of the origin of NCS character of these materials. The optical SHG intensity gradually decreases with increasing temperature, but no apparent NCS-to-CS phase transition is observed. TG/DTA (DTA = differential thermal analysis) measurements also did not indicate any specific phase transition in any of our materials (see Supporting Information, Figure S3). Since NCS arises from the ordering of Ge^{4+} and Te^{6+} cations in octahedral

DOI: 10.1021/acs.inorgchem.7b01013
Inorg. Chem. 2017, 56, 9019−9024

Table 3. Selected Bond Distances, Angles, and BVS for A(II)GeTeO$_6$ (A = Mn, Cd, Pb)

MnGeTeO$_6$			
cation	anion	bond length (Å)	BVS
Mn(1)	O(1)	2.1799(2) × 6	2.09 (Mn^{2+})
Ge(1)	O(1)	1.9008(1) × 6	3.97 (Ge^{4+})
Te(1)	O(1)	1.9913(1) × 6	5.77 (Te^{6+})
		angle (deg)	
Ge(1)−O(1)−Te(1)		95.6920(6)	
Mn(1)−O(1)−Ge(1)		131.1152(3)	
Mn(1)−O(1)−Te(1)		125.1152(3)	
CdGeTeO$_6$			
cation	anion	bond length (Å)	BVS
Cd(1)	O(1)	2.2898(1) × 6	2.12 (Cd^{2+})
Ge(1)	O(1)	1.8809(1) × 6	4.19 (Ge^{4+})
Te(1)	O(1)	1.9835(1) × 6	5.89 (Te^{6+})
		angle (deg)	
Ge(1)−O(1)−Te(1)		97.5529(4)	
Cd(1)−O(1)−Ge(1)		130.0619(2)	
Cd(1)−O(1)−Te(1)		124.5111(2)	
PbGeTeO$_6$			
cation	anion	bond length (Å)	BVS
Pb(1)	O(1)	2.5172(1) × 6	1.94 (Pb^{2+})
Ge(1)	O(1)	1.8865(1) × 6	4.13 (Ge^{4+})
Te(1)	O(1)	1.9894(1) × 6	5.80 (Te^{6+})
		angle (deg)	
Ge(1)−O(1)−Te(1)		98.5564(4)	
Pb(1)−O(1)−Te(1)		130.4564(2)	
Pb(1)−O(1)−Te(1)		125.1180(2)	

environment, the temperature-dependent SHG indicates that cation ordering improves with lower temperature, thus, the observation that the SHG intensity gradually decreases with increasing temperature. In the case of Cd and especially Pb compounds, there might be a saturation of SHG at low temperatures, which might indicate a long-range ordering temperature, for example, ∼300 °C for the Pb compound (Figure 4c); no such saturation temperature is evidenced for the Mn compound. Powder SHG measurement revealed SHG efficiencies of ∼0.37 and ∼0.21 times that of KDP for PbGeTeO$_6$ and CdGeTeO$_6$, respectively (see Figure 5). For MnGeTeO$_6$, we could not determine the SHG efficiency, due to its dark color, which absorbed the SHG signal.

Magnetic Behavior of MnGeTeO$_6$. The dc magnetic susceptibility of MnGeTeO$_6$ was measured under 1000 Oe in the temperature range of 2−300 K and is shown as χ and $1/\chi$ versus T plots in Figures 6 and 7, respectively. MnGeTeO$_6$ exhibits anti-ferromagnetic behavior with a Néel transition temperature (T_N) at ∼9.4 K. No significant divergence between zero field cooling (ZFC) and field cooling (FC) magnetization curves is observed. From the $1/\chi$ versus temperature shown in Figure 7, the susceptibility data were fit to the Curie−Weiss (CW) law, $\chi = C/(T-\theta)$ for $T > 25$ K, where C is the Curie constant, and θ is the Weiss constant: $C = 4.60$ emu K mol^{-1} and $\theta = -22.47$ K were extracted from the CW fit of the data. On the basis of the CW fit, the effective magnetic moment, $\mu_{eff} = 6.06\ \mu_B$/Mn is in good agreement with the theoretical spin only value for Mn^{2+} ($S = 5/2$, 5.92 μ_B). The negative Weiss constant indicates AFM interactions, which could arise from supersuper-exchange interactions of second-nearest neighbors Mn^{2+}−O^{2-}−Ge^{4+}−O^{2-}−Mn^{2+} and Mn^{2+}−O^{2-}−Te^{6+}−O^{2-}−Mn^{2+}.[31−33] In Figure S5, the isothermal magnetization of MnGeTeO$_6$ measured at 2 and 300 K as a function of applied field H at both temperatures are almost linear, which indicates that no ferromagnetic interaction is involved.

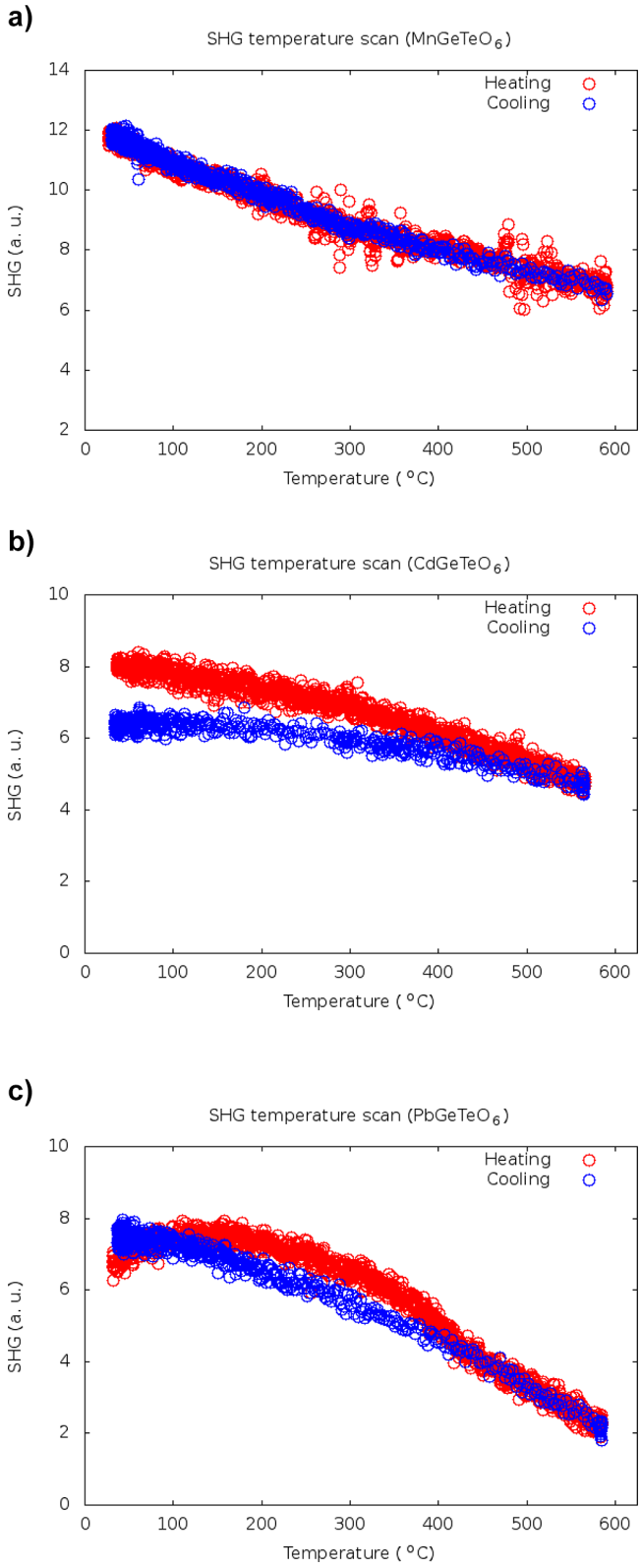

Figure 4. Temperature dependence of optical SHG intensity for A(II)GeTeO$_6$ (A = Mn, Cd, Pb) pellets between 0 and 600 °C: (a) MnGeTeO$_6$, (b) CdGeTeO$_6$, and (c) PbGeTeO$_6$.

DOI: 10.1021/acs.inorgchem.7b01013
Inorg. Chem. 2017, 56, 9019−9024

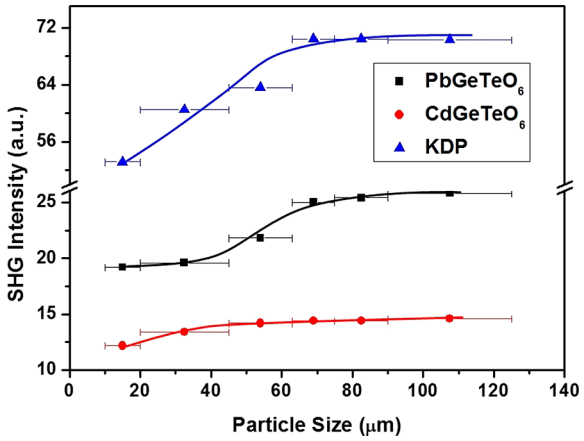

Figure 5. Phase matching, that is, particle size vs SHG intensity data for A(II)$GeTeO_6$ (A = Cd, Pb). KDP was used as an SHG reference material. The curve is drawn to guide the eye and is not a fit to the data.

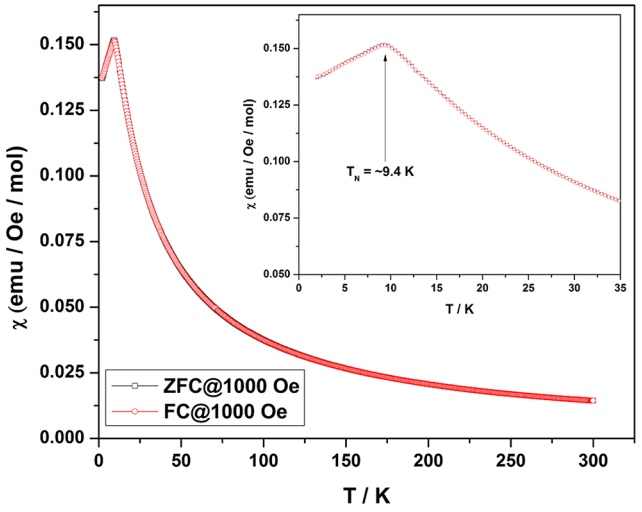

Figure 6. Temperature dependence of the magnetic susceptibility of $MnGeTeO_6$ measured in 1000 Oe. (inset) Enlargement of the low-temperature region revealing the ~9.4 K Néel temperature.

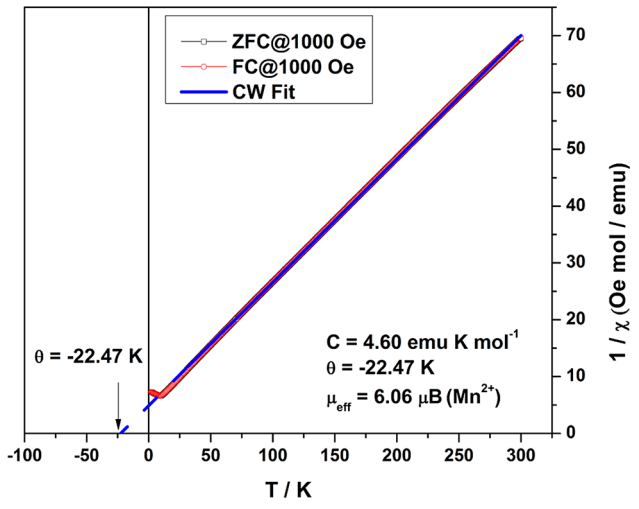

Figure 7. Inverse magnetic susceptibility of $MnGeTeO_6$ with a Curie–Weiss fit (solid line).

CONCLUSION

New non-centrosymmetric layered honeycomb tellurates A(II)$GeTeO_6$ (A = Mn, Cd, Pb) were successfully synthesized by a conventional solid-state reaction. A(II)$GeTeO_6$ exhibit a non-centrosymmetric two-dimensional honeycomb structure of $PbSb_2O_6$-type, and the ordering of Ge^{4+} and Te^{6+} in octahedral environment breaks the inversion symmetry. The size of A(II) cation in six coordination is an important factor to stabilize the $PbSb_2O_6$-based structure, and our experimental results indicate that the size of A cation should be larger than 0.8 Å. Second harmonic generation for A(II)$GeTeO_6$ confirmed the non-centrosymmetric character, and the materials exhibit relatively weak SHG responses compared to KDP (~0.37 and ~0.21 × KDP for $PbGeTeO_6$ and $CdGeTeO_6$, respectively). $MnGeTeO_6$ exhibits anti-ferromagnetic behavior with T_N of ~9.4 K with θ = −22.47 K.

We have demonstrated that non-centrosymmetric and magnetic phases may be designed from the centrosymetric parent $PbSb_2O_6$ in compositionally modified $ABB'O_6$-type compounds when the octahedrally coordinated B/B′ site cations are ordered. In addition the effective radius (>0.8 Å) of the A cation is also critical to stabilize non-centrosymmetric $PbSb_2O_6$-type structures. Further examples in these systems are in progress to confirm the correlations between B/B′ cation composition and arrangement and non-centrosymmetric property.

ASSOCIATED CONTENT

Supporting Information

The Supporting Information is available free of charge on the ACS Publications website at DOI: 10.1021/acs.inorgchem.7b01013.

Rietveld refinement plot of A(II)$GeTeO_6$ (A = Cd, Pb); trial synthesis of A(II)$GeTeO_6$ (A = Co, Ni, Cu, Pd) and their experimental PXRD; TG/DTA analysis for A(II)-$GeTeO_6$ (A = Mn, Cd, Pb) and PXRD after TGA measurement; isothermal magnetization of $MnGeTeO_6$ at 2 and 300 K as a function of applied field H (PDF)

Accession Codes

CCDC 1545374−1545376 contain the supplementary crystallographic data for this paper. These data can be obtained free of charge via www.ccdc.cam.ac.uk/data_request/cif, or by emailing data_request@ccdc.cam.ac.uk, or by contacting The Cambridge Crystallographic Data Centre, 12 Union Road, Cambridge CB2 1EZ, UK; fax: +44 1223 336033.

AUTHOR INFORMATION

Corresponding Author

*E-mail: martha@chem.rutgers.edu.

Author Contributions

The manuscript was written by contributions of all authors.

Notes

The authors declare no competing financial interest.

ACKNOWLEDGMENTS

This work was supported by NSF-DMR—1507252 grant. We thank Prof. P. Shiv Halasyamani (PSH) for powder SHG measurements. The contributions by P.S.H. and W.Z. were supported by the Welch Foundation, Grant No. E-1457 and the NSF DMR-1503573 grant.

DOI: 10.1021/acs.inorgchem.7b01013
Inorg. Chem. 2017, 56, 9019−9024

REFERENCES

(1) Auciello, O.; Scott, J. F.; Ramesh, R. The physics of ferroelectric memories. *Phys. Today* **1998**, *51*, 22−27.

(2) Damjanovic, D. Ferroelectric, dielectric and piezoelectric properties of ferroelectric thin films and ceramics. *Rep. Prog. Phys.* **1998**, *61*, 1267−1324.

(3) Halasyamani, P. S.; Poeppelmeier, K. R. Noncentrosymmetric Oxides. *Chem. Mater.* **1998**, *10*, 2753−2769.

(4) Saito, Y.; Takao, H.; Tani, T.; Nonoyama, T.; Takatori, K.; Homma, T.; Nagaya, T.; Nakamura, M. Lead-free piezoceramics. *Nature* **2004**, *432*, 84−87.

(5) Eerenstein, W.; Mathur, N. D.; Scott, J. F. Multiferroic and magnetoelectric materials. *Nature* **2006**, *442*, 759−765.

(6) Ra, H.-S.; Ok, K. M.; Halasyamani, P. S. Combining Second-Order Jahn-Teller Distorted Cations to Create Highly Efficient SHG Materials: Synthesis, Characterization, and NLO Properties of $BaTeM_2O_9$ (M = Mo^{6+} or W^{6+}). *J. Am. Chem. Soc.* **2003**, *125*, 7764−7765.

(7) Chang, H. Y.; Kim, S. W.; Halasyamani, P. S. Polar Hexagonal Tungsten Oxide (HTO) Materials: (1) Synthesis, Characterization, Functional Properties, and Structure-Property Relationships in $A_2(MoO_3)_3(SeO_3)$ (A = Rb^+ and Tl^+) and (2) Classification, Structural Distortions, and Second-Harmonic Generating Properties of Known Polar HTOs. *Chem. Mater.* **2010**, *22*, 3241−3250.

(8) Kim, Y. H.; Lee, D. W.; Ok, K. M. Strong Second Harmonic Generation (SHG) Originating from Combined Second-Order Jahn-Teller (SOJT) Distortive Cations in a New Noncentrosymmetric Tellurite, $InNb(TeO_4)_2$. *Inorg. Chem.* **2014**, *53*, 5240−5245.

(9) Cao, X.-L.; Hu, C.-L.; Kong, F.; Mao, J.-G. Explorations of New SHG Materials in the Alkali-Metal-Nb^{5+}-Selenite System. *Inorg. Chem.* **2015**, *54*, 10978−10984.

(10) Strayer, M. E.; Gupta, A. S.; Akamatsu, H.; Lei, S.; Benedek, N. A.; Gopalan, V.; Mallouk, T. E. Emergent Noncentrosymmetry and Piezoelectricity Driven by Oxygen Octahedral Rotations in n = 2 Dion-Jacobson Phase Layer Perovskites. *Adv. Funct. Mater.* **2016**, *26*, 1930−1937.

(11) Sen Gupta, A.; Akamatsu, H.; Brown, F. G.; Nguyen, M. A. T.; Strayer, M. E.; Lapidus, S.; Yoshida, S.; Fujita, K.; Tanaka, K.; Tanaka, I.; Mallouk, T. E.; Gopalan, V. Competing Structural Instabilities in the Ruddlesden-Popper Derivatives $HRTiO_4$ (R = Rare Earths): Oxygen Octahedral Rotations Inducing Noncentrosymmetricity and Layer Sliding Retaining Centrosymmetricity. *Chem. Mater.* **2017**, *29*, 656−665.

(12) Hill, R. J. Structure of lead antimonate ($PbSb_2O_6$) and its relationship to the crystal chemistry of lead dioxide in antimonial lead-acid batteries. *J. Solid State Chem.* **1987**, *71*, 12−18.

(13) Nakua, A. M.; Greedan, J. E. Structural and magnetic properties of transition metal arsenates, AAs_2O_6, A = Mn, Co, and Ni. *J. Solid State Chem.* **1995**, *118*, 402−411.

(14) Orosel, D.; Jansen, M. $PdAs_2O_6$, the first paramagnetic palladium oxide. *Z. Anorg. Allg. Chem.* **2006**, *632*, 1131−1133.

(15) Reehuis, M.; Saha-Dasgupta, T.; Orosel, D.; Nuss, J.; Rahaman, B.; Keimer, B.; Andersen, O. K.; Jansen, M. Magnetic properties of $PdAs_2O_6$: a dilute spin system with an unusually high Neel temperature. *Phys. Rev. B: Condens. Matter Mater. Phys.* **2012**, *85*, 115118.

(16) Koo, H.-J.; Whangbo, M.-H. Spin Exchange and Magnetic Dipole-Dipole Interactions Leading to the Magnetic Superstructures of MAs_2O_6 (M = Mn, Co, Ni). *Inorg. Chem.* **2014**, *53*, 3812−3817.

(17) Hiley, C. I.; Lees, M. R.; Fisher, J. M.; Thompsett, D.; Agrestini, S.; Smith, R. I.; Walton, R. I. Ruthenium(V) Oxides from Low-Temperature Hydrothermal Synthesis. *Angew. Chem., Int. Ed.* **2014**, *53*, 4423−4427.

(18) Tian, W.; Svoboda, C.; Ochi, M.; Matsuda, M.; Cao, H. B.; Cheng, J. G.; Sales, B. C.; Mandrus, D. G.; Arita, R.; Trivedi, N.; Yan, J. Q. High antiferromagnetic transition temperature of the honeycomb compound $SrRu_2O_6$. *Phys. Rev. B: Condens. Matter Mater. Phys.* **2015**, *92*, 100404.

(19) Woodward, P. M.; Sleight, A. W.; Du, L.-S.; Grey, C. P. Structural Stidies amd Ordrer-Disorder Phenomenon in a Series of New Quaternary Tellurates of the Type $A^{2+}M^{4+}Te^{6+}O_6$ and $A^{1+}M^{4+}Te^{6+}O_6$. *J. Solid State Chem.* **1999**, *147*, 99−116.

(20) Wulff, L.; Mueller-Buschbaum, H. Kagome layers connected by isolated trigonal SrO_6 prisms in the strontium manganate(IV) tellurate(VI). $SrMnTeO_6$. *Z. Naturforsch., B: J. Chem. Sci.* **1998**, *53*, 283−286.

(21) Kim, S. W.; Deng, Z.; Li, M.-R.; Sen Gupta, A.; Akamatsu, H.; Gopalan, V.; Greenblatt, M. PbMn(IV)TeO_6: A New Noncentrosymmetric Layered Honeycomb Magnetic Oxide. *Inorg. Chem.* **2016**, *55*, 1333−1338.

(22) Vats, B. G.; Phatak, R.; Krishnan, K.; Kannan, S. Preparation and structure of $BiCrTeO_6$: A new compound in Bi-Cr-Te-O system. Thermal expansion studies of Cr_2TeO_6, Bi_2TeO_6 and $BiCrTeO_6$. *Mater. Res. Bull.* **2013**, *48*, 3117−3121.

(23) Kim, S. W.; Deng, Z.; Fischer, Z.; Lapidus, S. H.; Stephens, P. W.; Li, M.-R.; Greenblatt, M. Structure and Magnetic Behavior of Layered Honeycomb Tellurates, BiM(III)TeO_6 (M = Cr, Mn, Fe). *Inorg. Chem.* **2016**, *55*, 10229−10237.

(24) Ivanov, S. A.; Mathieu, R.; Nordblad, P.; Tellgren, R.; Ritter, C.; Politova, E.; Kaleva, G.; Mosunov, A.; Stefanovich, S.; Weil, M. Spin and Dipole Ordering in Ni_2InSbO_6 and Ni_2ScSbO_6 with Corundum-Related Structure. *Chem. Mater.* **2013**, *25*, 935−945.

(25) Coelho, A. A. Indexing of powder diffraction patterns by iterative use of singular value decomposition. *J. Appl. Crystallogr.* **2003**, *36*, 86−95.

(26) Toby, B. H. EXPGUI, a graphical user interface for GSAS. *J. Appl. Crystallogr.* **2001**, *34*, 210−213.

(27) Kurtz, S. K.; Perry, T. T. Powder technique for the evaluation of nonlinear optical materials. *J. Appl. Phys.* **1968**, *39*, 3798−3813.

(28) Ok, K. M.; Chi, E. O.; Halasyamani, P. S. Bulk characterization methods for non-centrosymmetric materials: second-harmonic generation, piezoelectricity, pyroelectricity, and ferroelectricity. *Chem. Soc. Rev.* **2006**, *35*, 710−717.

(29) Brown, I. D.; Altermatt, D. Bond-valence parameters obtained from a systematic analysis of the inorganic crystal structure database. *Acta Crystallogr., Sect. B: Struct. Sci.* **1985**, *B41*, 244−247.

(30) Brown, I. D. Recent Developments in the Methods and Applications of the Bond Valence Model. *Chem. Rev.* **2009**, *109*, 6858−6919.

(31) Goodenough, J. B. Theory of the Role of Covalence in the Perovskite-Type Manganites [La, M(II)]MnO_3. *Phys. Rev.* **1955**, *100*, 564.

(32) Anderson, P. W. New approach to the theory of superexchange interactions. *Phys. Rev.* **1959**, *115*, 2−13.

(33) Goodenough, J. B. *Magnetism and the Chemical Bond*; Interscience: New York, 1963.

DOI: 10.1021/acs.inorgchem.7b01013
Inorg. Chem. 2017, 56, 9019−9024